Earth and Planetary Science Letters 507 (2019) 10–20

Contents lists available at ScienceDirect

Earth and Planetary Science Letters

www.elsevier.com/locate/epsl

Area and volume of mid-latitude glacier-like forms on Mars

Stephen Brough [a,b,*], Bryn Hubbard [a], Alun Hubbard [a,c]

[a] Department of Geography and Earth Sciences, Aberystwyth University, Aberystwyth, UK
[b] School of Geography, Politics and Sociology, Newcastle University, Newcastle, UK
[c] Centre for Arctic Gas Hydrate, Environment and Climate, Department of Geology, University of Tromsø, Tromsø, Norway

ARTICLE INFO

Article history:
Received 15 August 2017
Received in revised form 26 September 2018
Accepted 21 November 2018
Available online 4 December 2018
Editor: W.B. McKinnon

Keywords:
Mars
glaciation
glacier
water
climate change
GIS

ABSTRACT

Although a substantial ice cover has been identified within the mid-latitudes of Mars, there is uncertainty regarding the formation, current and former volume, and dynamic evolution of these ice masses. Here, we present the first comprehensive ice volume estimate of martian glacier-like forms (GLFs) from systematic population scale mapping and volumetric analysis. The outlines of 1243 GLFs were manually delineated from 6 m per pixel Context Camera (CTX) images and the volume of each determined using a volume–area scaling approach. Our results show that GLFs cover a surface area of 11344 ± 393 km^2 and have a total volume of 1744 ± 441 km^3. Using two end-member scenarios for ice concentration by volume of 30% (pore ice) and 90% (debris-covered glacier ice), we calculate the volume of ice contained within GLFs to be between 523 ± 132 km^3 (480 ± 121 Gt) and 1570 ± 397 km^3 (1439 ± 364 Gt), equivalent to a mean global water layer 3 to 10 mm thick. We investigate the local topographic setting of each GLF by reference to the Mars Orbiter Laser Altimeter (MOLA) digital elevation model. Our analysis reveals that globally GLFs are on average larger in latitudes >36° and on slopes between 2 and 8°. In the northern hemisphere GLFs between 500 and 2500 m in elevation and in the southern hemisphere GLFs with a northern aspect are also larger on average. The observed spatial patterns of GLF landform and volume distribution suggests that regional to local meteorological and topographical conditions play an important role in GLF ice accumulation and/or preservation. Assuming a net accumulation rate of 10 mm a^{-1} typical of climatic excursions with high obliquity, we estimate a period of at least 13 ka is required to yield the average calculated GLF ice thickness of ~130 m. Such a period is well within the timeframe of a high obliquity cycle (20–40 ka), suggesting that the current GLF volume could have formed during a single climate excursion.

1. Introduction

Extensive evidence has been presented for the existence and character of buried water ice within Mars' mid-latitudes (~30–60°) (e.g. Squyres, 1978, 1979; Squyres and Carr, 1986; Head et al., 2003; Mustard et al., 2001; Milliken et al., 2003; Arfstrom and Hartmann, 2005; Levy et al., 2007, 2014; Dickson et al., 2008; Holt et al., 2008; Head et al., 2010; Dickson et al., 2012; Souness et al., 2012; Hartmann et al., 2014). Pervasive landforms consistent with viscous deformation and the resulting flow of ice are of particular interest. Collectively, these landforms have been termed viscous flow features, or VFFs (Milliken et al., 2003; Souness et al., 2012). Among some of the earliest VFFs identified were lobate debris aprons (LDA – Squyres, 1978, 1979), lineated valley fill (LVF – Squyres, 1978, 1979), and concentric crater fill (CCF – Squyres and Carr, 1986). The original interpretations of these landforms were that they were either ice-assisted (<30% ice) or were formed by debris/talus flows from ground ice emplaced by vapour diffusion (e.g. Squyres, 1978, 1979). However, more recent investigations – corroborated with geophysical evidence showing many, if not all, of these landforms are composed of a substantial core (~90%) of water ice (Holt et al., 2008; Plaut et al., 2009) – have noted several similarities between VFFs and debris-covered glaciers on Earth (e.g. Head et al., 2010; Mackay and Marchant, 2017).

Given that under present-day conditions ground ice is generally only stable at latitudes above ~45° (Mellon and Jakosky, 1995; Mellon et al., 2004), many of these ice-rich landforms are located in regions where such ice is predicted to be unstable. It has therefore been hypothesised that VFFs are relict landforms, that formed as a result of climatic excursions redistributing ice from polar to mid-latitude regions during periods of high (>30°) obliquity (Head et al., 2003; Forget et al., 2006; Madeleine et al., 2009;

* Corresponding author at: School of Geography, Politics and Sociology, Daysh Building, Newcastle University, Newcastle upon Tyne, NE1 7RU, UK.
E-mail address: stephen.brough@ncl.ac.uk (S. Brough).

https://doi.org/10.1016/j.epsl.2018.11.031
0012-821X/

Fassett et al., 2014). VFF survival to the present day is therefore considered to be due principally to the ice being protected from sublimation by surface debris (Holt et al., 2008; Fastook et al., 2014). It is not currently clear how continuous or episodic such periods of ice accumulation were in order for VFFs to form, or how this may have varied spatially at the planetary scale. Constraining the timing and length of time required for VFF formation is hindered by the fact that numerical models can only satisfactorily predict orbital variations for approximately the last 20 Ma (e.g. Laskar et al., 2004) and many VFFs show evidence of ablation and ice mass loss since emplacement (e.g. Dickson et al., 2008; Brough et al., 2016a). It is therefore likely that VFF formation reflects a complex history of ice accumulation and loss (e.g. Fastook et al., 2014; Parsons and Holt, 2016). Nonetheless, crater-related age estimates for LDA, LVF and CCF constrain the age of formation to between 60 Ma and 1 Ga years ago (see Berman et al., 2015). Furthermore, ice volume estimates from analysis of mapped outlines of >11,000 mid-latitude VFFs (LDA, LVF, CCF), suggest that a total of between 1.25×10^5 and 3.74×10^5 km^3 of ice is held within these landforms – the equivalent of a global water layer 0.8–2.4 m thick (Levy et al., 2014; Karlsson et al., 2015). Thus, VFFs (i) constitute an important component of the surface/near-surface water inventory of Mars (Carr and Head, 2015), and (ii) have become an important proxy for improving our understanding of long term climate change throughout Mars' Amazonian Epoch (e.g. Fassett et al., 2014; Fastook et al., 2014; Parsons and Holt, 2016).

In recent years, growing attention has focused on a set of smaller scale VFFs that, in planform, appear similar to (debris-covered) valley glaciers or rock glaciers on Earth (e.g. Milliken et al., 2003; Arfstrom and Hartmann, 2005; Hubbard et al., 2011, 2014; Souness et al., 2012). Such landforms have become known as glacier-like forms, or GLFs (Hubbard et al., 2011), noting that these landforms have also been subject to a range of nomenclature within the literature, including: viscous flow features (Milliken et al., 2003), glacier-like flows (Arfstrom and Hartmann, 2005), superposed lineated valley fill (Levy et al., 2007), and small-scale superposed lineated valley fill (Levy et al., 2007). GLFs appear to flow downslope, generally coalescing from cirque-like alcoves or valleys to a narrow elongate tongue that is commonly demarcated by raised latero-terminal ridges. The identification of such ridges suggests that GLFs are relict remains of more extensive ice masses that have receded since a climatic optimum (Hubbard et al., 2011; Hartmann et al., 2014; Brough et al., 2016a), perhaps as a result of the last major change from a high (∼35°) to low (∼25°) mean obliquity period ∼4 Ma–6 Ma BP (Laskar et al., 2004). Although identified in isolation, GLFs often feed into pre-existing VFFs to form what Head et al. (2010) described as Mars' integrated glacial landsystem.

In total ∼1300 GLFs have been identified between 25 and 65° latitude in both hemispheres and inter-hemispheric similarities in their morphology (e.g. length and width) and environmental settings suggests a common evolutionary history (Souness et al., 2012; Brough et al., 2016a). Age estimates for several GLFs in Crater Greg, although somewhat speculative due to the small areas involved and thus numbers of craters used (e.g. Dauber et al., 2013), indicate that they are likely <10 Ma old, with an upper boundary of <50 Ma (Arfstrom and Hartmann, 2005; Hartmann et al., 2014). Furthermore, numerous studies have noted a distinct stratigraphic relationship between GLFs and other ice-rich landforms (LDA, LVF and CCF), with the former being superposed on the latter (e.g. Levy et al., 2007). The apparent younger age of GLFs and their stratigraphic relationships with other ice-rich landforms has provided supporting evidence for the hypothesis that GLFs represent a more recent, perhaps localised and small-scale, glacial phase and the more extensive LDA, LVF and CCF deposits record an earlier, regional, glacial phase (Levy et al., 2007; Dickson et al., 2008; Brough et al., 2016b). Therefore, GLFs may represent (i) important archives of geologically recent climatic change (e.g. Hartmann et al., 2014; Brough et al., 2016a), (ii) an active/recently active hydrological store, and (iii) significant landscaping agents since GLFs are the highest-altitude component of Mars' glacial valley landsystem. Despite these important questions, and unlike the wider LDA, LVF and CCF deposits (e.g. Levy et al., 2014; Karlsson et al., 2015), no population-scale outline mapping or estimation of the water ice volume of GLFs exist and our understanding of the basic physical and mechanical properties of GLFs are still being investigated (e.g. Souness et al., 2012; Hubbard et al., 2014; Brough et al., 2016a). The study by Souness et al. (2012) represents the most comprehensive analysis of GLFs to date, providing the geographic coordinates and morphometric data for each individual GLF identified at the time. However, this analysis was conducted on the basis of point measurements and/or geometric buffers (rectangles/circles from MOLA-derived background topography) rather than from directly mapped GLF boundaries.

The aim of this paper is to advance understanding of the glacial history of Mars' GLFs by providing the first population-scale outline mapping and estimation of the water ice volume of GLFs, as well as evaluating controls over the resulting volume distribution. Specifically, we provide (i) manually digitised outlines for all GLFs; (ii) an estimate of the volume of water ice held within GLFs, using a volume–area scaling approach commonly applied to ice masses on Earth (cf. Bahr et al., 2015 and references therein) and more recently to Mars (Karlsson et al., 2015); (iii) an assessment of potential controlling environmental variables on GLF volume; and (iv) an updated GLF inventory to that of Souness et al. (2012).

2. Data and methods

2.1. Data sets

Analysis of GLFs in this study was based on all 1293 landforms identified in the database of Souness et al. (2012).[1] This database contained two pieces of information used in the present study: (i) the Context Camera (CTX) image ID, and (ii) the location (latitude and longitude) of all GLFs. Where a GLF had been identified, map projected (level 2) CTX images at 6 m pixel resolution were produced using the USGS' Integrated Software for Imagers and Spectrometers. The processed CTX images, GLF centroid coordinates and a gridded digital elevation model (DEM) from the Mars Orbiter Laser Altimeter (MOLA), were then analysed in ESRI ArcMap (v 10.1). MOLA elevation data at ∼463 m horizontal resolution was used to define a number of topographic related parameters including slope and aspect (in radians and broken down into linear sine and cosine form).

2.2. GLF outline mapping and area calculation

GLF outlines (vector polygons) were manually digitised by a single user (SB) at a scale of 1:25000 following the criteria set out in Souness et al. (2012) and summarised in Table 1. Three scenarios were identified and classified in demarcating the GLF boundaries (Fig. 1). Type 1 GLFs ($n = 249$) were the easiest to demarcate, terminating on a non-ice surface and with their complete boundary being constrained by the surrounding topography (e.g., Fig. 1a, d). Type 2 GLFs ($n = 216$) are similar to Type 1 but differ in that they terminate within a wider icy terrain, often superposed on the

[1] Souness et al. (2012) originally identified 1309 GLFs. However, Brough et al. (2016a) recently refined this number to 1293 due to the identification of duplicate entries.

Table 1
Criteria for GLF identification following Souness et al. (2012).

	Description
[i]	Be surrounded by topography showing general evidence of flow over or around obstacles
[ii]	Be distinct from the surrounding landscape exhibiting a texture or colour difference from adjacent terrains
[iii]	Display surface foliation indicative of down-slope flow; e.g. compressional/extensional ridges, surface lineations, arcuate surface morphologies or surface crevassing
[iv]	Have a length to width ratio >1 (i.e. be longer than it is wide)
[v]	Have either a discernible 'head' or a discernible 'terminus' indicating a compositional boundary or process threshold
[vi]	Appear to contain a volume of ice (or some other viscous substance), having a flat 'valley fill' surface, thus differentiating it from a previously glaciated 'GLF skeleton'

wider LDA/LVF (e.g., Fig. 1b, e). Type 3 GLFs ($n = 778$) similarly terminate in wider icy terrain but do not have an unequivocal continuous boundary (e.g., Fig. 1c, f). In this scenario, the boundary is identified based on observable changes in surface texture as indicated by criterion [ii] of Table 1.

Compound GLFs (i.e. where two or more GLFs share a border) were treated as follows. GLFs flowing in different directions from a common source area were each classified separately and mapped from the drainage divide (Fig. SF1 in Supplementary Material). In contrast, ice flow units originating from separate source areas and converging into a single distinct terminus (e.g. Fig. SF1) were classified as a single GLF. In all scenarios, when the GLF margin was flanked by a moraine-like ridge (MLR) the boundary was placed on the inside of the MLR. If multiple MLRs were visible then the innermost ridge was used. Once the outline of the GLF had been mapped, any internal bedrock/nunatak perturbations were removed from the GIS polygon.

Each GLF was assigned to the unique ID corresponding to Souness et al. (2012), with GLFs that here are treated as one, rather than multiple entries, assigned the first corresponding ID. Subsequently, the area for each GLF was calculated in ArcMap using an Albers Equal Area Conic map projection.

2.3. GLF volume calculation

Knowledge of the composition and ice thickness distribution of GLFs on Mars is severely limited and difficult to obtain using currently available satellite-based geophysical methods (Hubbard et al., 2014). Numerous methods for estimating ice volume exist for ice masses on Earth (see Farinotti et al., 2017). However, the more sophisticated of these require input data not presently available for Mars (e.g., surface velocity; mass balance; high-resolution DEMs). Here we applied a simple and commonly used volume–area scaling method (cf. Bahr et al., 2015 and references therein) based solely on (glacier) area.

Volume–area scaling rests on the principle that (glacier) volume (V) can be estimated from the (glacier) surface area (A) with the relationship: $V = kA^{\Upsilon}$ or $\log(V) = \log(k) + \Upsilon \log(A)$, where k and Υ are scaling parameters derived from data, or through theoretical considerations (Bahr et al., 2015). Although a number of regional and global volume–area scaling relationships have been proposed for glaciers on Earth (see Bahr et al., 2015), given the general absence of ancillary data, volume–area scaling relationships for martian ice masses are scant and, to our knowledge, the only scaling relationship for mid-latitude VFFs is provided by Karlsson et al. (2015). Based on radar-validated measurements of ice thickness from LDAs on Mars, Karlsson et al. (2015) determined a volume–area relationship: $\log(V) = 1.12 \log(A) - 0.978$. Although obtained from LDA, in the absence of contemporaneous radar-validated measurements for GLFs, we adopted this relationship and applied it to our outline mapping (see Section 2.2) to calculate the volume for each individual GLF.

2.4. GLF inventory attributes

2.4.1. Environmental parameters

As well as the ID, Type, area and volume values already attributed to each GLF (see Sections 2.2 and 2.3), several environmental parameters were calculated from the MOLA topographic datasets (see Section 2.1) including: the centroid x–y coordinates; elevations of maximum, minimum, mean, median and standard

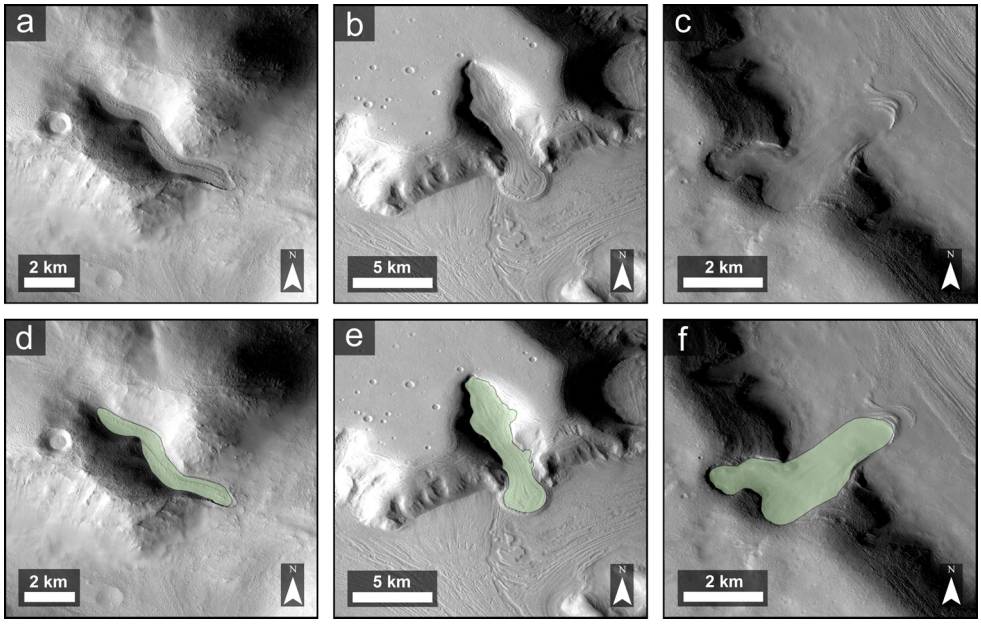

Fig. 1. Examples of GLFs (a)–(c) and their manually digitized outlines (d)–(f). (a) A Type 1 GLF. The boundary is readily demarcated with the GLF constrained within a valley and the terminus identified by moraine-like ridges (Subset of CTX image B04_011261_2146_XN_34N289W; centred on ~70.59°E, 33.12°N). (b) A Type 2 GLF. The boundary is again clear, but in this case the GLF is superposed on LVF (Subset of CTX image P22_009653_2224_XN_42N309W; centred on ~50.50°E, 42.24°N). (c) A Type 3 GLF. The boundary is somewhat unclear as the GLF emerges out of the alcove and merges with the outer LVF deposit (Subset of CTX image P03_002112_2208_XN_40N337W; centred on ~22.27°E, 40.07°N). (For interpretation of the colours in the figure, the reader is referred to the web version of this article.)

deviation; mean slope; and the mean aspect (also classified into eight cardinal and inter-cardinal directions).[2] The mean aspect for each GLF was derived following Paul (2007) and the resulting orientations were classified into 45° bins corresponding to the eight cardinal and inter-cardinal directions. The mapped GLF outlines and corresponding environmental parameters are provided as Supplementary Material.

2.4.2. Analysis of environmental parameters

Several environmental parameters were extracted and analysed to evaluate controls over GLF volume. Mean GLF volume (km^3) was calculated as a function of longitude (°), latitude (°), aspect (cardinal and inter-cardinal directions), slope (°) and elevation (m relative to Mars datum), and Welch's t-tests were run, using an alpha (P) level of 0.05, to assess for significant differences between populations (Table ST1 in Supplementary Material). Global and hemispheric GLF counts and total GLF volume were also plotted and can be found in Supplementary Material to this manuscript (Figs. SF2–SF5 and Tables ST2–ST6).

2.5. Uncertainty in GLF mapping and volume calculation

2.5.1. Outline mapping

Manual classification is prone to errors that reflect a user's ability to identify the features of interest (Smith, 2011). Glacier boundaries, and particularly those of debris-covered glaciers, are inherently difficult to define from remotely-sensed imagery alone (e.g. Paul et al., 2013). However, these difficulties can be mitigated to some degree by a single interpreter following a consistent and tightly constrained mapping technique in terms of e.g., criteria and scale (Smith, 2011), both of which were followed in the present study (see Section 2.2).

In order to quantify uncertainty associated with this study's outline mapping, we followed standard procedure (e.g. Paul et al., 2013) and conducted an error analysis by performing multiple and independent digitisations of a selection of GLFs. Each of the three GLF Types (see Section 2.2) presented in Fig. 1 was digitised independently at a scale of 1:25 000 five times, and the resulting GLF areas were compared. This yielded, a mean standard deviation of 2.0, 2.2 and 4.0% of the area for Types 1, 2 and 3 GLFs respectively. The uncertainty in the total mapped GLF area reported in this study was consequently calculated by applying these Type-dependant (1 std. dev.) variations to each individual GLF as appropriate.

2.5.2. Volume estimation

Karlsson et al. (2015) constrained their volume–area relationship by interpolating multiple Shallow Radar (SHARAD) transects into 3D bed elevation maps for seven LDAs, allowing their volumes to be approximated. By analysing misfit between their interpolated bed elevation maps and individual SHARAD tracks, Karlsson et al. (2015) attributed an uncertainty of 25% to their calibration data set. In the absence of SHARAD data for GLFs – which are generally too small for the bed to register without substantial valley-side echoes – we adopt this value and add it to the area uncertainty of 2.0, 2.2 and 4.0% to Type 1, 2 and 3 GLFs respectively (see Section 2.5.1).

Our volume estimates may also be subject to additional unconstrained sources of uncertainty. Many of the LDAs from which Karlsson's volume–area scaling relationship was derived appeared to have a relatively shallow bed. Since ice thickness generally scales inversely with bed slope and larger glaciers tend to have lower mean slopes than smaller glaciers (Cuffey and Paterson, 2010), volumes are likely overestimated for the GLFs studied herein. In contrast, Bahr et al. (2015) noted that the volume–area method tends to underestimate actual volume when applied to only a part or subsection of a glacier. Given that part of the boundary of Type 3 GLFs in this study is connected to another ice body (Fig. 1c), our volume estimation in such cases is likely to be too small. Furthermore, the generalised nature of volume–area scaling renders it more appropriate for population-scale analyses (such as our application herein) than for specific individual cases (see review by Bahr et al., 2015). For example, applying a universal value of k to a large population of glaciers was found by Bahr et al. (2015) to yield an accurate net volume, while applying it to a single randomly-selected glacier led to a volume error (expressed as 1 standard deviation) of ∼34%. Given the challenges of obtaining data (e.g. radar) that is able to resolve these sources of uncertainty, combined with the likely range of differing conditions across Mars' GLF population, it is currently impossible to quantify overall uncertainty and we therefore use that adopted by Karlsson et al. (2015) for larger VFFs.

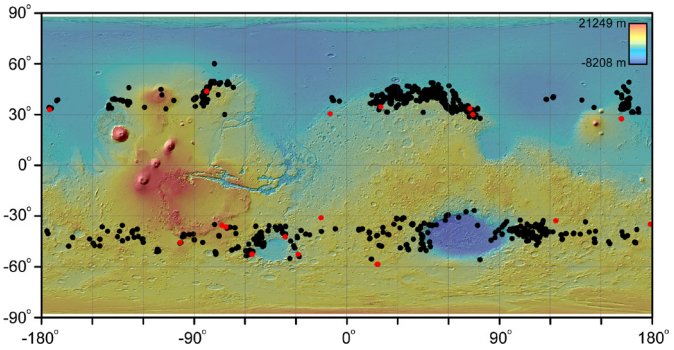

Fig. 2. Map of Mars showing the mid-latitude distribution of each mapped GLF (black dots). 1243 GLFs were mapped globally: 698 were located in the northern hemisphere and 545 were located in the southern hemisphere. Red dots identify the locations of the 20 GLFs not mapped in this study. Background map is MOLA elevation transparency overlain on a MOLA hillshade projection. (For interpretation of the colours in the figure, the reader is referred to the web version of this article.)

3. Results

3.1. GLF outline mapping

From a total population of 1293 GLFs identified by Souness et al. (2012), we positively identified 1273 (∼98%) of them, with the remaining 20 being either unidentifiable or repeated GLFs in the earlier inventory. Mapping these 1273 GLFs resulted in 1243 unique entries, with 30 compound GLFs being re-classified as single GLFs. Of the total number of 1243 mapped GLFs, 698 (∼56%) are located in the northern hemisphere and 545 (∼44%) in the southern hemisphere (Fig. 2).

3.2. GLF area

In total, the 1243 GLFs identified have a surface area of 11344 ± 393 km^2 (Table 2), equivalent to 0.01% of the total surface area of Mars. Of this surface area, 6680 ± 240 km^2 (∼59%) is in the northern hemisphere and 4664 ± 154 km^2 (∼41%) is in the southern hemisphere (Table 2). Global mean GLF area is 9.13 km^2 (std. dev. = 18.69), comprising 9.57 km^2 (std. dev. = 21.78) and 8.56 km^2 (std. dev. = 13.76) in the northern and southern hemispheres, respectively (Table 2).

[2] Many of the environmental parameters described above formed part of the study by Souness et al. (2012). Our intention was not to replicate but to update the inventory of Souness et al. (2012) based on directly mapped, rather than approximated, outlines of individual GLFs. Herein, we only report on new findings obtained from this study or through results obtained from previously unreported analysis.

Table 2
Basic descriptive statistics for GLF area and volume.

ROI	Area				Volume			
	Total (km^2)	Total (%)	Mean (km^2)	Std. dev.	Total (km^3)	Total (%)	Mean (km^3)	Std. dev.
Global	11343.93	100.0	9.13	18.69	1743.60	100.0	1.40	3.54
North	6679.75	58.9	9.57	21.78	1045.10	59.9	1.50	4.22
South	4664.17	41.1	8.56	13.76	698.49	40.1	1.28	2.41

3.3. GLF volume

The following analyses were carried out in terms of GLF volume only but, given the scaling method applied, similar relationships apply to GLF area.

3.3.1. Population-scale volume distribution

3.3.1.1. Spatial distribution by volume We calculate the total martian GLF volume to be 1744 ± 441 km^3 (Table 2). Of this volume, 1045 ± 265 km^3 (~60%) is in the northern hemisphere and 698 ± 175 km^3 (~40%) is in the southern hemisphere (Table 2). Global mean GLF volume is 1.40 km^3 (std. dev. = 3.54), comprising 1.50 km^3 (std. dev. = 4.22) and 1.28 km^3 (std. dev. = 2.41) in the northern and southern hemispheres, respectively (Table 2).

Several regions show high volumetric contributions, including the 'fretted terrain' of the northern hemisphere and regions surrounding the Hellas impact basin in the southern hemisphere (Figs. 3 and SF4). This distribution broadly reflects the overall GLF population (Fig. SF2): mean GLF volume in these regions is similar to the hemispheric GLF mean (Fig. 3). However, there are two regions where mean GLF volume has a statistically significant difference from the respective hemispheric mean; these are Tempe Terra (between −95 and −65° longitude) in the northern hemisphere ($P = 0.023$) and surrounding the Argyre impact basin (between −65 and −20° longitude) in the southern hemisphere ($P = 0.016$), where mean GLF volume increases to 2.85 and 2.31 km^3, respectively (Fig. 3 and Table ST1).

3.3.1.2. Size-class distribution by volume The distribution of GLFs by count and total volume for selected size classes is summarised in Table ST7 of Supplementary Material and the normalised (%) distribution presented in Fig. 4. Globally, the distribution appears to be dominated by middle size-class GLFs, with ~87% of the total count and ~55% of the total volume contained within GLFs of volume 0.1–5 km^3. The two smallest size classes for volume (e.g. GLFs <0.1 km^3) host ~8% of the total count but contain <1% of the total volume. In contrast, only ~5% of GLFs are in the two largest size classes for volume (e.g. GLFs >5 km^3), but they contribute ~45% of the total volume (Fig. 4a and Table ST7). On the whole, GLF size-class distribution is similar for both hemispheres (Fig. 4b–c and Table ST7).

3.3.2. Environmental controls over GLF volume distribution

3.3.2.1. Latitude Mean GLF volume increases with latitude such that GLFs located <36° north or south have mean volumes of 0.98 and 0.62 km^3 respectively, compared to mean volumes of 1.69 and 1.42 km^3 for those located >36° (Fig. 5a and Table ST3). This difference in mean volume between GLFs located <36° and GLFs located >36° is statistically significant for both the northern ($P = 0.006$) and southern hemispheres ($P =< 0.001$), thus revealing those lower-latitude GLFs are on average smaller than those GLFs at higher-latitudes. This association is particularly strong in the southern hemisphere, where mean GLF volume increases to 3.27 km^3 at latitudes >48° (Fig. 5a and Table ST3).

3.3.2.2. Aspect In both hemispheres GLFs flowing towards the north (NW, N, NE) are larger than those flowing towards the south (SE, S, SW) (Fig. 5b–d and Table ST4). In the northern hemisphere GLFs with a northern aspect have a mean volume of 1.55 km^3 in contrast to a mean volume of 1.19 km^3 for GLFs with a southern aspect. This difference is stronger in the southern hemisphere where GLFs have mean volumes of 1.91 and 1.10 km^3 for northern and southern aspects, respectively. However, a statistically significant difference in mean volume between northern and southern flowing GLFs is noted only for the southern hemisphere ($P = 0.024$).

3.3.2.3. Slope Mean GLF volume peaks on slopes between 2 and 4° in both the northern and southern hemispheres (Fig. 5e–g and Table ST5). In both hemispheres, there is a statistically significant difference in mean volume between GLFs located on 2–8° slopes and GLFs located on slopes outside the range of 2–8° ($P =< 0.001$), with the former having larger mean volumes of 2.94 and 2.46 km^3 and the latter having smaller mean volumes of 0.71 and 0.95 km^3 for the northern and southern hemispheres, respectively. This association is enhanced in the northern hemisphere where a mean GLF volume of 7.13 km^3 is noted for GLFs on slopes between 2 and 4° (Fig. 5e–g and Table ST5). Plotting mean slope against GLF size (Fig. 6) reveals that smaller GLFs show greater variability in slope than larger GLFs, which have lower and less variable slopes.

3.3.2.4. Elevation Two elevation ranges host GLFs of increased mean volume, between −3500 and −2000 m, with a mean GLF volume of 1.86 km^3, and between 500 and 2500 m, with a mean GLF volume of 1.67 km^3 (Fig. 5h–j and Table ST6). Although these peaks are visible in both the northern and southern hemisphere, it does mask an inter-hemispheric contrast: in the northern hemisphere the mean GLF volume is greatest between 500 and 2500 m (3.73 km^3) and in the southern hemisphere mean GLF volume is greatest between −3500 and −2000 m (2.99 km^3). However, this difference in mean GLF volume is only statistically significant for those northern hemispheric GLFs between 500 and 2500 m ($P = 0.049$).

4. Interpretation and discussion

4.1. GLF volume distribution and contribution to mid-latitude ice

Globally, GLF volume is distributed similarly to the parent GLF population (Figs. 3 and SF2), with several regions of high volume concentration along the martian dichotomy boundary, Tempa Terra and Phlegra Montes in the northern hemisphere and to the east of the Hellas impact basin in the southern hemisphere. This spatial distribution is similar to the wider volume distribution of VFFs (LDA and LVF) in the mid-latitudes of Mars (e.g. Levy et al., 2014), indicating similarity in controls on GLF and VFF formation and/or preservation. Coupled with the observed spatial variation in GLF volume (Figs. 3 and 4), these observations add further support to the hypothesis that regional to local meteorological and topographical conditions play an important role in VFF formation due to ice accumulation and preservation (Dickson et al., 2012; Levy et al., 2014; Brough et al., 2016a), and it is not exclusively

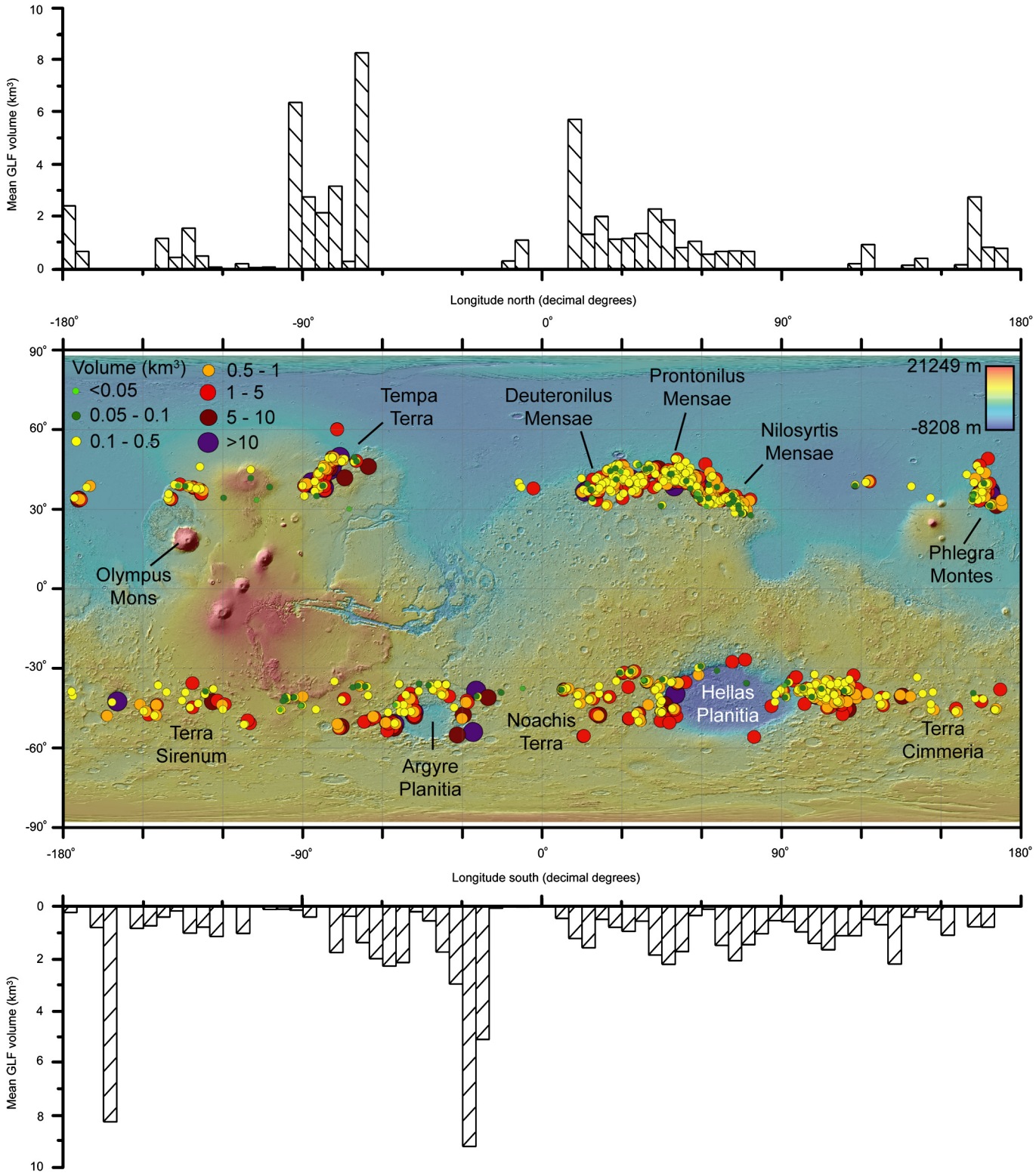

Fig. 3. Map of Mars showing the mid-latitude distribution of individual GLF volume. The colour and size of the circles represents the volume (km^3) of each GLF (green through to purple; larger circles = more volume). GLF volume is 1743.60 km^3 globally: 1045.10 km^3 is in the northern hemisphere and 698.49 km^3 is in the southern hemisphere. Bar plots, showing mean GLF volume in 5° longitude bins, for each hemisphere are presented above and below the distribution map. Background map as in Fig. 2. (For interpretation of the colours in the figure, the reader is referred to the web version of this article.)

a result of latitude-dependent insolation forcing. Under this scenario, specific atmospheric circulation patterns, driven by changes in orbital parameters, strongly influence the locations where glacial conditions persist, and would be a possible explanation for the spatial heterogeneity noted in the distribution of GLFs.

Our estimated mid-latitude GLF volume of 1744 ± 441 km^3 does not take into account variations in the ice content of those GLFs. The ice content of Earth's rock glaciers varies widely, as does their proposed internal structure and mode of formation (e.g., Martin and Whalley, 1987). Haeberli et al. (2006) summa-

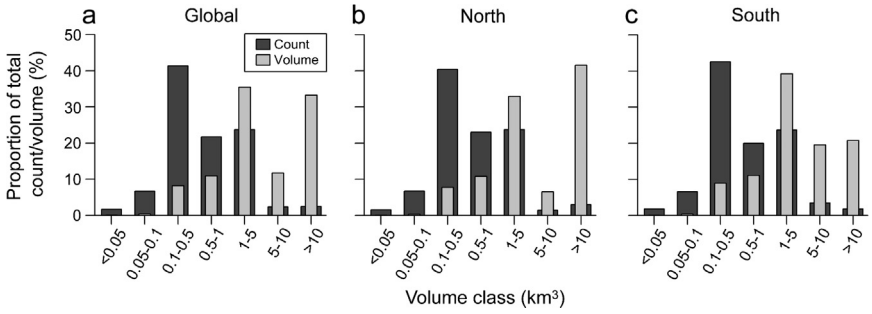

Fig. 4. GLF count and volume per size class for: (a) global, (b) northern hemisphere, and (c) southern hemisphere GLF populations.

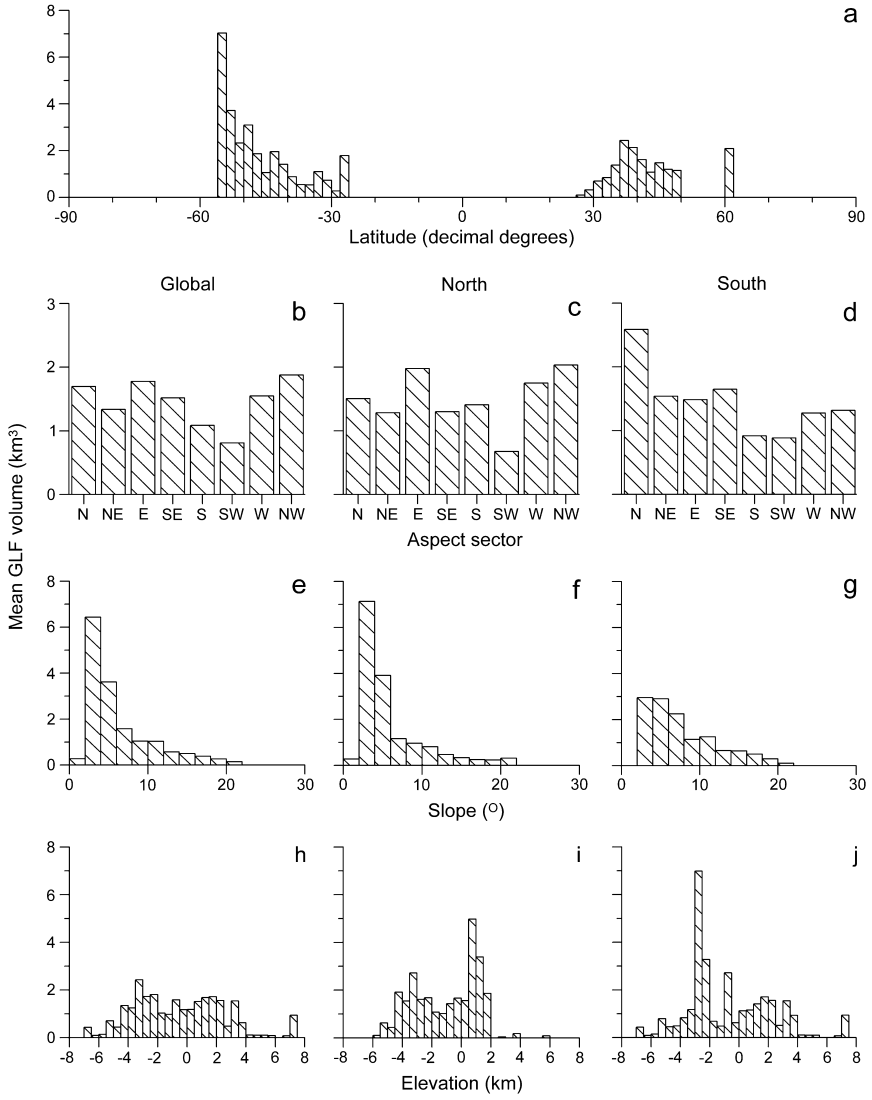

Fig. 5. Bar plots showing mean GLF volume (km^3) for: (a) global and hemispheric latitude in 2° bins; (b) global, (c) northern and (d) southern hemispheric aspect in the eight cardinal and inter-cardinal directions; (e) global, (f) northern and (d) southern hemispheric slope in 2° bins; (h) global, (i) northern hemisphere and (j) southern hemisphere elevation in 500 m bins.

rized measured ice contents within active rock glaciers as typically being between 40 and 70% by volume (their Table 3). Consistent with these studies, we follow the ice concentrations considered appropriate for martian VFFs by Levy et al. (2014), using two end member scenarios. Scenario 1 favours a low ice content value of 30% by volume, as suggested by the ice-assisted debris/rock glacier origin (e.g. Squyres, 1978, 1979). Scenario 2 favours a high ice content value of 90% by volume, as suggested by the debris-covered glacier origin (e.g. Holt et al., 2008; Head et al., 2010). These two end member scenarios yield ice contributions of 523 ± 132 km^3 (480 ± 121 Gt) and 1570 ± 397 km^3 (1439 ± 364 Gt) for mid-latitude GLFs, or the equivalent of a global water layer between 3 ± 1 and 10 ± 3 mm thick. Although it is unlikely that all GLFs, and by extension VFFs, are compositionally homogeneous (e.g. Parson et al., 2011), converging evidence from morphological (Head et al., 2010), geophysical (Holt et al., 2008; Plaut et al., 2009) and numerical (Forget et al., 2006; Madeleine et al., 2009; Fastook et al., 2014) studies points towards

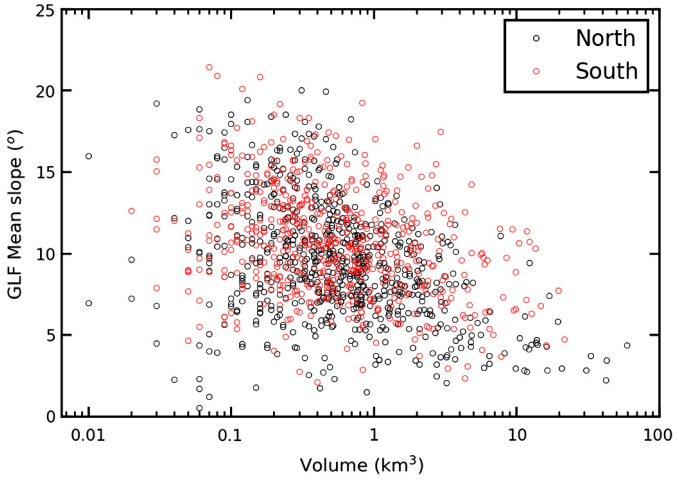

Fig. 6. Scatter plot showing GLF volume against mean GLF slope for each individual GLF. The distribution reveals inter-hemispheric similarity between the northern (black open circles) and southern hemispheres (red open circles). (For interpretation of the colours in the figure, the reader is referred to the web version of this article.)

VFF formation through the accumulation of atmospherically derived ice. We therefore favour the (higher) debris-covered glacier ice volume estimate of 1570 ± 397 km^3 (1439 ± 364 Gt).

The VFF inventory of Levy et al. (2014), although being the most comprehensive to date, did not include GLFs in their ice volume estimation. Thus, the contribution of mid-latitude VFFs to the present day surface/near-surface water budget should be revised upwards to account for this. We note the concurrence of some 130 GLFs mapped in this inventory and those identified as part of the wider VFF analysis by Levy et al. (2014). These 130 GLFs have an estimated ice volume of 606 ± 154 km^3. Therefore, the remaining 1203 GLFs add an additional ice volume of between 341 ± 86 and 1024 ± 258 km^3 to the VFF estimate of Levy et al. (2014), based on our two end member scenarios.

Comparing the volume of GLFs (on the order of 10^3 km^3) to other ice deposits located in Mars' mid-latitudes (Table 3) reveals that they contribute about an order of magnitude less (on the order of 10^4 km^3) than the latitude-dependent mantle (Mustard et al., 2001; Kreslavsky and Head, 2002; Conway and Balme, 2014), LVF and CCF, and are of about two orders of magnitude less (on the order of 10^5 km^3) than LDA (Levy et al., 2014; Karlsson et al., 2015). In total, GLFs contribute an additional ice volume of ∼0.4% to Mars' currently known mid-latitude deposits. On a global scale, GLFs contain <0.1% of the volume of ice stored in the polar ice caps (Table 3), thereby contributing only a minor component to the present day surface/near-surface water budget (e.g. Carr and Head, 2015). However, taking into account the degraded nature of many GLFs (Brough et al., 2016a), it is possible that they once contributed a much larger volume to Mars' water budget. Furthermore, given that GLFs are the highest-altitude component of Mars' glacial valley landsystem, they likely constitute an important component to the erosion and supply of debris in mid-latitude environments (Levy et al., 2016) and, given their Late Amazonian age, may represent some of the most recent geomorphological activity on Mars (Hubbard et al., 2014; Brough et al., 2016a).

4.2. Geologic context of GLF volume

4.2.1. Latitude

Latitude exerts a systematic control over GLF volume, with all identified GLFs being located between 25 and 65° north and south. Within this range, GLF volume tends to increase with increasing latitude, particularly above ∼36°, and is most noticeable in the southern hemisphere, where a prominent peak is located between 50 and 60° (Fig. 5a and Table ST3). We propose that this distribution reflects two processes. First, initial ice emplacement during a high-obliquity phase, as modelled by Madeleine et al. (2009), includes both a similar range to that of the GLFs analysed herein and shows a notable peak in the relatively high latitudes (40–60°) of the southern hemisphere in particular. To a large extent, therefore, we interpret the spatial distribution of our reconstructed GLF volumes to reflect that of initial ice emplacement. Second, shallow ground ice is currently increasingly unstable at latitudes below ∼40–45° (Mellon and Jakosky, 1995; Mellon et al., 2004). Thus, since their initial formation, low-latitude GLFs have likely been subject to preferential ablation relative to higher latitude GLFs, as identified by Brough et al. (2016a).

4.2.2. Aspect

Although, as expected, pole-ward facing GLFs predominate in the southern hemisphere (Souness et al., 2012; Fig. SF3), these GLFs are smaller and contain less mass on average than those facing north (Fig. 5d). In terrestrial scenarios pole-ward facing alcoves are often preferential locations for ice accumulation and/or preservation due to reduced insolation (Unwin, 1973). However, our observations of southern-hemisphere equator-facing GLFs being on average larger than pole-ward facing GLFs contradicts this pattern, but may be consistent with reversals during the high-obliquity events that have been invoked for their formation. Further, it is likely that local meteorological and topographical conditions can play an important role in ice accumulation and preservation (Dickson et al., 2012; Levy et al., 2014; Brough et al., 2016a).

4.2.3. Slope

GLFs located on slopes between 2 and 8° have the largest average volume (Fig. 5e–g and Table ST5). The influence of slope on glacier thickness on Earth is well-established and shows that larger glaciers tend to have lower mean slopes and smaller glaciers tend to have steeper slopes, principally due to the influence of slope on driving stress and hence velocity (Cuffey and Paterson, 2010). Thus, slope process may have a similar influence on martian GLFs as their Earth based counterparts.

In terms of the relationship between mean slope and GLF size (Fig. 6), the increase in the variability of slope values for smaller

Table 3
Ice volume estimates and global equivalent water layer thickness for several mid-latitude landforms. The two polar caps are included for comparison.

Landform	Ice volume (km^3)	Global equivalent water layer (m)	References
Glacier-like forms	0.52–1.57 × 10^3	0.003–0.010	This study
North Polar Cap	0.82–1.14 × 10^6	5.2–7.2	Smith et al., 2001; Putzig et al., 2009
South Polar Cap	1.20–1.70 × 10^6	7.6–10.8	Zubar et al., 1998; Plaut et al., 2007
Lobate debris aprons	0.79–2.36 × 10^5	0.50–1.50	Levy et al., 2014; Karlsson et al., 2015
Concentric crater fill	2.63–7.88 × 10^4	0.17–0.50	Levy et al., 2014
Lineated valley fill	1.95–5.86 × 10^4	0.12–0.37	Levy et al., 2014
Latitude-dependent mantle	1.00–8.00 × 10^4	0.06–0.51	Mustard et al., 2001; Kreslavsk and Head, 2002; Conway and Balme, 2014

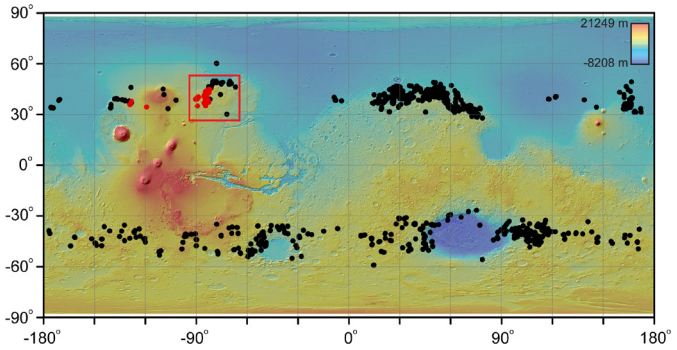

Fig. 7. Map of Mars showing the distribution of northern hemisphere GLFs between 500 and 2500 m in elevation (red dots [$n = 34$]) relative to the overall GLF population (black dots). For the northern hemisphere, GLFs in this elevation range are larger in volume than GLFs outside of this elevation range. Note the predominance of GLFs in the Tempa Terra region (red box). (For interpretation of the colours in the figure, the reader is referred to the web version of this article.)

GLFs reveals that smaller GLFs are less sensitive to their topographic settings than larger GLFs, implying that smaller GLFs can form in a wider range of terrain. A similar effect has been reported in relation to the topographic setting of glaciers in the European Alps on Earth (e.g. Paul et al., 2011). As a consequence, the increased topographic variability observed for small GLFs may affect their response to current/future climatic perturbations, such that small GLFs of similar size may show variable responses to the same climatic perturbation.

4.2.4. Elevation

Mean GLF volume is noticeably larger between the elevations of 500 and 2500 m in the northern hemisphere, suggesting this zone holds some influence over GLF volume (Fig. 5h–j and Table ST6). Plotting the distribution of these larger northern hemisphere GLFs indicates that they cluster around Tempa Terra (Fig. 7). This suggests that GLF volume may be related to a combination of both elevation and local to regional meteorological conditions providing favourable conditions for ice accumulation and/or preservation. Indeed, large-scale martian atmospheric modelling indicates that high net ice accumulation is predicted in Tempa Terra under high obliquity conditions (e.g. Madeleine et al., 2009).

4.3. Implications for Late Amazonian glaciation on Mars

Age estimates place GLFs as young surface landforms <50 Ma and likely <10 Ma old (Arfstrom and Hartmann, 2005; Hartmann et al., 2014), but our understanding of when or for how long glacial conditions are required for GLF formation is uncertain. A mean ice thickness of ~130 m was calculated from the area and volume of each GLF in our analysis. Under a 10 mm a^{-1} accumulation rate possible during climatic excursions of high obliquity (e.g. Madeleine et al., 2009), ice of this thickness could have accumulated within ~13 ka assuming no influent mass from beyond GLF boundaries. Considering each high obliquity excursion, which were common prior to ~300 Ka ago, lasts on the order of 20–40 Ka (Laskar et al., 2002; Head et al., 2003) it is possible that Mars' current GLF volume could have been emplaced during a single event – as suggested for the associated latitude-dependant mantle (Conway and Balme, 2014). However, as ~33% of the GLF population shows evidence of ablation and mass loss (Brough et al., 2016a) it is likely that a more complex formation history exists, perhaps requiring multiple high obliquity accumulation cycles, a scenario proposed to explain the formation of some larger VFFs (e.g. Parsons and Holt, 2016). Considering it has been estimated that over 15 high obliquity periods occurred during the last 2 Ma (Laskar et al., 2002; Head et al., 2003), such a scenario is plausible and indeed, likely (e.g. Milliken et al., 2003). Therefore, the timespan for formation of ~13 ka should be viewed as a minimum. As with the wider VFF deposits (e.g. Fastook et al., 2014; Parsons and Holt, 2016), constraining the environmental conditions and timespan required to form GLFs can be tested with numerical ice flow models if appropriate boundary conditions are known and is a direction for future research.

5. Summary and conclusions

A new population-scale GLF inventory was compiled through a combination of MOLA topographic data and directly mapped outlines of 1243 GLFs from CTX imagery. We used these products to (i) provide the first ice volume estimate of GLFs to the mid-latitude surface/near surface water budget on Mars; (ii) improve our understanding of the controls on GLF formation and evolution; and (iii) assess their formation in relation to the most recent high obliquity climatic excursions on Mars. From these investigations, we conclude the following:

- GLF area was calculated to be 11344 ± 393 km^2, equivalent to ~0.01% of the total surface area of Mars. Of this surface area, 6680 ± 240 km^2 (~59%) is in the northern hemisphere and 4664 ± 154 km^2 (~41%) is in the southern hemisphere.
- GLF volume was calculated to be 1744 ± 441 km^3. Using two end member scenarios the actual population-scale ice volume contribution is found to be 523 ± 132 km^3 (480 ± 121 Gt) for a pore ice content (30% ice by volume) scenario and 1570 ± 397 km^3 (1439 ± 364 Gt) for a debris-covered glacier (90% ice by volume) scenario. This mapped out to a global equivalent water layer of between 3 ± 1 and 10 ± 3 mm thick. Based on converging morphological, geophysical and numerical evidence pointing towards GLF/VFF formation through the accumulation of atmospherically derived ice, we favour the (higher) debris-covered glacier estimate.
- GLF deposits represent an ice volume contribution on the order of 10^3 km^3, between one and two orders of magnitude less than those reported for LDM, LDA, LVF and CCF (Mustard et al., 2001; Kreslavsky and Head, 2002; Conway and Balme, 2014; Levy et al., 2014; Karlsson et al., 2015). GLFs contribute an equivalent of 0.4% of currently known mid-latitude ice deposits.
- Coupling mean thickness estimates with GCM derived ice accumulation rates (e.g. Madeleine et al., 2009) suggests that GLFs require at least 13 ka to obtain the equivalent mass currently stored in these features. This places a minimum boundary on the duration of ice emplacement that is less than one high-obliquity cycle. However, we do not rule out the possibility that formation requires multiple depositional cycles and suggest that better understanding the required formation conditions for GLFs be a priority research area.
- Spatial patterns of GLF landform and volume distribution suggest that regional to local meteorological and topographical conditions play an important role in GLF ice accumulation and preservation. Specifically, given the observed zonal pattern in distribution, GLF location and volume, although influenced by, is not simply a relation of latitudinal dependence or insolation driven factors. Further, variations in physical environments are also important in providing microclimates favourable for the accumulation and/or preservation of ice.
- Assessment of the environmental conditions that influence GLF accumulation and/or preservation revealed that GLF size is, to a certain extent, controlled by their physical setting. Specifically, GLFs globally are on average larger in latitudes >36° and on slopes between 2 and 8°. In the northern hemisphere GLFs between 500 and 2500 m in elevation and in the south-

ern hemisphere GLFs with a northern aspect are also larger on average.

Acknowledgements

SB gratefully acknowledges support from Aberystwyth University through a Doctoral Career Development Scholarship. AH gratefully acknowledges support from the Research Council of Norway through its Centres of Excellence funding scheme, project number 223259. We are grateful to Souness et al. (2012) and Levy et al. (2014) for making their inventory data, analysed within this study, freely available. We thank the Editor William McKinnon and reviewer Robert Craddock for their helpful and insightful comments.

Appendix A. Supplementary material

Supplementary material related to this article can be found online at https://doi.org/10.1016/j.epsl.2018.11.031.

References

Arfstrom, J., Hartmann, W.K., 2005. Martian flow features, moraine-like ridges, and gullies: terrestrial analogs and interrelationships. Icarus 174 (2), 321–335. https://doi.org/10.1016/j.icarus.2004.05.026.

Bahr, D.B., Pfeffer, W.T., Kaser, G., 2015. A review of volume–area scaling of glaciers. Rev. Geophys. 53 (1), 95–140. https://doi.org/10.1002/2014RG000470.

Berman, D.C., Crown, D.A., Joseph, E.C.S., 2015. Formation and mantling ages of lobate debris aprons on Mars: insights from categorized crater counts. Planet. Space Sci. 111, 83–99. https://doi.org/10.1016/j.pss.2015.03.013.

Brough, S., Hubbard, B., Hubbard, A., 2016a. Former extent of glacier-like forms on Mars. Icarus 274, 37–49. https://doi.org/10.1016/j.icarus.2016.03.006.

Brough, S., Hubbard, B., Souness, C., Grindrod, P.M., Davis, J., 2016b. Landscapes of polyphase glaciation: eastern Hellas Planitia, Mars. J. Maps 12 (3), 530–542. https://doi.org/10.1080/17445647.2015.1047907.

Carr, M.H., Head, J.W., 2015. Martian surface/near-surface water inventory: sources, sinks, and changes with time. Geophys. Res. Lett. 42 (3), 726–732. https://doi.org/10.1002/2014gl062464.

Conway, S.J, Balme, M.R., 2014. Decameter thick remnant glacial ice deposits on Mars. Geophys. Res. Lett. 41 (15), 2014GL060314. https://doi.org/10.1002/2014gl060314.

Cuffey, K.M., Paterson, W.S.B., 2010. The Physics of Glaciers, 4th ed. Butterworth-Heinemann, Oxford.

Daubar, I.J., McEwen, A.S., Byrne, S., Kennedy, M.R., Ivanov, B., 2013. The current martian cratering rate. Icarus 225 (1), 506–516. https://doi.org/10.1016/j.icarus.2013.04.009.

Dickson, J.L., Head, J.W., Marchant, D.R., 2008. Late Amazonian glaciation at the dichotomy boundary on Mars: evidence for glacial thickness maxima and multiple glacial phases. Geology 36 (5), 411. https://doi.org/10.1130/g24382a.1.

Dickson, J.L., Head, J.W., Fassett, C.I., 2012. Patterns of accumulation and flow of ice in the mid-latitudes of Mars during the Amazonian. Icarus 219 (2), 723–732. https://doi.org/10.1016/j.icarus.2012.03.010.

Farinotti, D., Brinkerhoff, D.J., Clarke, G.K.C., Fürst, J.J., Frey, H., Gantayat, P., Gillet-Chaulet, F., Girard, C., Huss, M., Leclercq, P.W., Linsbauer, A., Machguth, H., Martin, C., Maussion, F., Morlighem, M., Mosbeux, C., Pandit, A., Portmann, A., Rabatel, A., Ramsankaran, R.A.A.J., Reerink, T.J., Sanchez, O., Stentoft, P.A., Kumari, S.S., van Pelt, W.J.J., Anderson, B., Benham, T., Binder, D., Dowdeswell, J.A., Fischer, A., Helfricht, K., Kutuzov, S., Lavrentiev, I., McNabb, R., Gudmundsson, G.H., Li, H., Andreassen, L.M., 2017. How accurate are estimates of glacier ice thickness? Results from ITMIX, the ice thickness models intercomparison eXperiment. Cryosphere 11 (2), 949–970. https://doi.org/10.5194/tc-11-949-2017.

Fassett, C.I., Levy, J.S., Dickson, J.L., Head, J.W., 2014. An extended period of episodic northern mid-latitude glaciation on Mars during the Middle to Late Amazonian: implications for long-term obliquity history. Geology 42 (9), 763–766. https://doi.org/10.1130/g35798.1.

Fastook, J.L., Head, J.W., Marchant, D.R., 2014. Formation of lobate debris aprons on Mars: assessment of regional ice sheet collapse and debris-cover armoring. Icarus 228, 54–63. https://doi.org/10.1016/j.icarus.2013.09.025.

Forget, F., Haberle, R.M., Montmessin, F., Levrard, B., Head, J.W., 2006. Formation of glaciers on Mars by atmospheric precipitation at high obliquity. Science 311 (5759), 368–371. https://doi.org/10.1126/science.1120335.

Haeberli, W., Hallet, B., Arenson, L., Elconin, R., Humlum, O., Kääb, A., Kaufman, V., Ladanyi, B., Matsuoka, N., Springman, S., Mühll, D.V., 2006. Permafrost creep and rock glacier dynamics. Permafr. Periglac. Process. 17, 189–214. https://doi.org/10.1002/ppp.561.

Hartmann, W.K., Ansan, V., Berman, D.C., Mangold, N., Forget, F., 2014. Comprehensive analysis of glaciated martian crater Greg. Icarus 228, 96–120. https://doi.org/10.1016/j.icarus.2013.09.016.

Head, J.W., Mustard, J.F., Kreslavsky, M.A., Milliken, R.E., Marchant, D.R., 2003. Recent ice ages on Mars. Nature 426 (6968), 797–802. https://doi.org/10.1038/Nature02114.

Head, J.W., Marchant, D.R., Dickson, J.L., Kress, A.M., Baker, D.M., 2010. Northern mid-latitude glaciation in the Late Amazonian period of Mars: criteria for the recognition of debris-covered glacier and valley glacier landsystem deposits. Earth Planet. Sci. Lett. 294 (3–4), 306–320. https://doi.org/10.1016/j.epsl.2009.06.041.

Holt, J.W., Safaeinili, A., Plaut, J.J., Head, J.W., Phillips, R.J., Seu, R., Kempf, S.D., Choudhary, P., Young, D.A., Putzig, N.E., Biccari, D., Gim, Y., 2008. Radar sounding evidence for buried glaciers in the Southern Mid-Latitudes of Mars. Science 322 (5905), 1235–1238. https://doi.org/10.1126/science.1164246.

Hubbard, B., Souness, C., Brough, S., 2014. Glacier-like forms on Mars. Cryosphere 8 (6), 2047–2061. https://doi.org/10.5194/tc-8-2047-2014.

Hubbard, B., Milliken, R.E., Kargel, J.S., Limaye, A., Souness, C., 2011. Geomorphological characterisation and interpretation of a mid-latitude glacier-like form: Hellas Planitia, Mars. Icarus 211 (1), 330–346. https://doi.org/10.1016/j.icarus.2010.10.021.

Karlsson, N.B., Schmidt, L.S., Hvidberg, C.S., 2015. Volume of Martian midlatitude glaciers from radar observations and ice flow modeling. Geophys. Res. Lett. 42 (8), 2015GL063219. https://doi.org/10.1002/2015gl063219.

Kreslavsky, M.A., Head, J.W., 2002. Mars: nature and evolution of young latitude-dependent water-ice-rich mantle. Geophys. Res. Lett. 29 (15). https://doi.org/10.1029/2002gl015392.

Laskar, J., Levrard, B., Mustard, J.F., 2002. Orbital forcing of the martian polar layered deposits. Nature 419 (6905), 375–377. https://doi.org/10.1038/Nature01066.

Laskar, J., Correia, A.C.M., Gastineau, M., Joutel, F., Levrard, B., Robutel, P., 2004. Long term evolution and chaotic diffusion of the insolation quantities of Mars. Icarus 170 (2), 343–364. https://doi.org/10.1016/j.icarus.2004.04.005.

Levy, J.S., Head, J.W., Marchant, D.R., 2007. Lineated valley fill and lobate debris apron stratigraphy in Nilosyrtis Mensae, Mars: evidence for phases of glacial modification of the dichotomy boundary. J. Geophys. Res. 112 (E8). https://doi.org/10.1029/2006je002852.

Levy, J.S., Fassett, C.I., Head, J.W., 2016. Enhanced erosion rates on Mars during Amazonian glaciation. Icarus 264, 213–219. https://doi.org/10.1016/j.icarus.2015.09.037.

Levy, J.S., Fassett, C.I., Head, J.W., Schwartz, C., Watters, J.L., 2014. Sequestered glacial ice contribution to the global Martian water budget: geometric constraints on the volume of remnant, midlatitude debris-covered glaciers. J. Geophys. Res., Planets 119 (10), 2014JE004685. https://doi.org/10.1002/2014je004685.

Mackay, S.L., Marchant, D.R., 2017. Obliquity-paced climate change recorded in Antarctic debris-covered glaciers. Nat. Commun. 8, 14194. https://doi.org/10.1038/ncomms14194.

Madeleine, J.B., Forget, F., Head, J.W., Levrard, B., Montmessin, F., Millour, E., 2009. Amazonian northern mid-latitude glaciation on Mars: a proposed climate scenario. Icarus 203 (2), 390–405. https://doi.org/10.1016/j.icarus.2009.04.037.

Martin, H.M., Whalley, W.B., 1987. Rock glaciers part 1: rock glacier morphology: classification and distribution. Prog. Phys. Geogr. 11 (2), 260–282. https://doi.org/10.1177/030913338701100205.

Mellon, M.T., Jakosky, B.M., 1995. The distribution and behavior of Martian ground ice during past and present epochs. J. Geophys. Res., Planets 100 (E6), 11781–11799. https://doi.org/10.1029/95je01027.

Mellon, M.T., Feldman, W.C., Prettyman, T.H., 2004. The presence and stability of ground ice in the southern hemisphere of Mars. Icarus 169 (2), 324–340. https://doi.org/10.1016/j.icarus.2003.10.022.

Milliken, R.E., Mustard, J.F., Goldsby, D.L., 2003. Viscous flow features on the surface of Mars: observations from high-resolution Mars Orbiter Camera (MOC) images. J. Geophys. Res., Planets 108 (E6). https://doi.org/10.1029/2002je002005.

Mustard, J.F., Cooper, C.D., Rifkin, M.K., 2001. Evidence for recent climate change on Mars from the identification of youthful near-surface ground ice. Nature 412 (6845), 411–414. https://doi.org/10.1038/35086515.

Parsons, R., Holt, J., 2016. Constraints on the formation and properties of a Martian lobate debris apron: insights from high-resolution topography, SHARAD radar data, and a numerical ice flow model. J. Geophys. Res., Planets 121 (3), 432–453. https://doi.org/10.1002/2015je004927.

Parsons, R., Nimmo, F., Miyamoto, H., 2011. Constraints on martian lobate debris apron evolution and rheology from numerical modeling of ice flow. Icarus 214 (1), 246–257. https://doi.org/10.1016/j.icarus.2011.04.014.

Paul, F., 2007. The New Swiss Glacier Inventory 2000 – Application of Remote Sensing and GIS. Schriftenreihe Physische Geographie. Universitat Zurich.

Paul, F., Frey, H., Le Bris, R., 2011. A new glacier inventory for the European Alps from Landsat TM scenes of 2003: challenges and results. Ann. Glaciol. 52 (59), 144–152.

Paul, F., Barrand, N.E., Baumann, S., Berthier, E., Bolch, T., Casey, K., Frey, H., Joshi, S.P., Konovalov, V., Le Bris, R., Molg, N., Nosenko, G., Nuth, C., Pope, A., Racoviteanu, A., Rastner, P., Raup, B., Scharrer, K., Steffen, S., Winsvold, S., 2013. On the accuracy of glacier outlines derived from remote-sensing data. Ann. Glaciol. 54 (63), 171–182. https://doi.org/10.3189/2013AOG63A296.

Plaut, J.J., Safaeinili, A., Holt, J.W., Phillips, R.J., Head, J.W., Seu, R., Putzig, N.E., Frigeri, A., 2009. Radar evidence for ice in lobate debris aprons in the mid-northern latitudes of Mars. Geophys. Res. Lett. 36 (2). https://doi.org/10.1029/2008gl036379.

Plaut, J.J., Picardi, G., Safaeinili, A., Ivanov, A.B., Milkovich, S.M., Cicchetti, A., Kofman, W., Mouginot, J., Farrell, W.M., Phillips, R.J., Clifford, S.M., Frigeri, A., Orosei, R., Federico, C., Williams, I.P., Gurnett, D.A., Nielsen, E., Hagfors, T., Heggy, E., Stofan, E.R., Plettemeier, D., Watters, T.R., Leuschen, C.J., Edenhofer, P., 2007. Subsurface radar sounding of the south polar layered deposits of Mars. Science 316 (5821), 92–95. https://doi.org/10.1126/science.1139672.

Putzig, N.E., Phillips, R.J., Campbell, B.A., Holt, J.W., Plaut, J.J., Carter, L.M., Egan, A.F., Bernardini, F., Safaeinili, A., Seu, R., 2009. Subsurface structure of Planum Boreum from Mars Reconnaissance Orbiter Shallow Radar soundings. Icarus 204 (2), 443–457. https://doi.org/10.1016/j.icarus.2009.07.034.

Smith, D.E., Zuber, M.T., Frey, H.V., Garvin, J.B., Head, J.W., Muhleman, D.O., Pettergill, G.H., Phillips, R.J., Solomon, S.C., Zwally, H.J., Banerdt, W.B., Duxbury, T.C., Golombek, M.P., Lemoine, F.G., Neumann, G.A., Rowlands, D.D., Aharonson, O., Ford, P.G., Ivanov, A.B., Johnson, C.L., McGovern, P.J., Abshire, J.B., Afzal, R.S., Sun, X., 2001. Mars Orbiter Laser Altimeter: experiment summary after the first year of global mapping of Mars. J. Geophys. Res., Planets 106 (E10), 23689–23722. https://doi.org/10.1029/2000je001364.

Smith, M.J., 2011. Digital mapping: visualisation, interpretation and quantification of landforms. In: Smith, M.J., Paron, P., Griffiths, J. (Eds.), Geomorphological Mapping: Methods and Applications. Elsevier, Oxford, pp. 225–251.

Souness, C., Hubbard, B., Milliken, R.E., Quincey, D., 2012. An inventory and population-scale analysis of martian glacier-like forms. Icarus 217 (1), 243–255. https://doi.org/10.1016/j.icarus.2011.10.020.

Squyres, S.W., 1978. Martian fretted terrain – flow of erosional debris. Icarus 34 (3), 600–613. https://doi.org/10.1016/0019-1035(78)90048-9.

Squyres, S.W., 1979. Distribution of lobate debris aprons and similar flows on Mars. J. Geophys. Res. 84, 8087–8096. https://doi.org/10.1029/Jb084ib14p08087.

Squyres, S.W., Carr, M.H., 1986. Geomorphic evidence for the distribution of ground ice on Mars. Science 231 (4735), 249–252. https://doi.org/10.1126/science.231.4735.249.

Unwin, D.J., 1973. The distribution and orientation of corries in Northern Snowdonia, Wales. Trans. Inst. Br. Geogr. 58, 85–97. https://doi.org/10.2307/621583.

Zuber, M.T., Smith, D.E., Solomon, S.C., Abshire, J.B., Afzal, R.S., Aharonson, O., Fishbaugh, K., Ford, P.G., Frey, H.V., Garvin, J.B., Head, J.W., Ivanov, A.B., Johnson, C.L., Muhleman, D.O., Neumann, G.A., Pettengill, G.H., Phillips, R.J., Sun, X., Zwally, H.J., Banerdt, W.B., Duxbury, T.C., 1998. Observations of the north polar region of Mars from the Mars Orbiter Laser Altimeter. Science 282 (5396), 2053–2060. https://doi.org/10.1126/science.282.5396.2053.